

# Characterising natural bedform morphology and its influence on flow

Alice Lefebvre<sup>1</sup> · Andries J. Paarlberg<sup>2</sup> · Christian Winter<sup>1</sup>

Received: 3 May 2016 / Accepted: 8 June 2016 / Published online: 14 June 2016  
© Springer-Verlag Berlin Heidelberg 2016

**Abstract** Bedforms such as dunes and ripples are ubiquitous in rivers and coastal seas, and commonly described as triangular shapes from which height and length are calculated to estimate hydrodynamic and sediment dynamic parameters. Natural bedforms, however, present a far more complicated morphology; the difference between natural bedform shape and the often assumed triangular shape is usually neglected, and how this may affect the flow is unknown. This study investigates the shapes of natural bedforms and how they influence flow and shear stress, based on four datasets extracted from earlier studies on two rivers (the Rio Paraná in Argentina, and the Lower Rhine in The Netherlands). The most commonly occurring morphological elements are a sinusoidal stoss side made of one segment and a lee side made of two segments, a gently sloping upper lee side and a relatively steep (6 to 21°) slip face. A non-hydrostatic numerical model, set up using Delft3D, served to simulate the flow over fixed bedforms with various morphologies derived from the identified morphological elements. Both shear stress and turbulence increase with increasing slip face angle and are only marginally affected by the dimensions and positions of the upper and lower lee side. The average slip face angle determined from the bed profiles is 14°, over which there is no permanent flow separation. Shear stress and turbulence above natural bedforms are higher than above a flat bed but much lower than over the often assumed 30° lee side angle.

## Introduction

In rivers and marine environments, the transport of sediment frequently generates rhythmic wavy features on the bed. The dimensions and dynamics of these bedforms both reflect and influence hydrodynamic and sediment dynamics processes at various spatiotemporal scales. For instance, bedform size and migration reflect the nature and intensity of sediment transport (e.g. Villard and Kostaschuk 1998; Ernstsen et al. 2005; Barnard et al. 2011). It is thus essential to precisely characterise bedform morphology and dynamics in order to correctly estimate and forecast transport rates and morphological changes. Indeed, bedforms have a strong influence on flow (see reviews of Best 2005; Venditti 2013, and references therein), especially through flow acceleration over the bedform stoss side and deceleration/reversal over the lee side, formation of macroturbulence in the lee of bedforms, and form roughness. A good understanding and precise characterisation of flow over bedforms is therefore relevant for system understanding, and the modelling and prediction of riverine and marine hydrodynamics and sediment transport.

To date, most studies on the physical and numerical modelling of bedforms have investigated the dynamics and effects of angle-of-repose bedforms, i.e. bedforms with a lee side angle of at least 30°. However, it is now recognised that many large rivers and coastal environments are characterised by bedforms with lee side slopes lower than the angle of repose, the so-called low-angle bedforms (Best 2005). Furthermore, laboratory and numerical experiments have concentrated on bedforms of relatively simple geometry, typically a triangular or sinusoidally shaped stoss side and straight lee side (“sine-straight” shape; e.g. Smith and McLean 1977; Engel 1981; Nelson et al. 1993; McLean et al. 1994; Bennett and Best 1995; Venditti and Bennett 2000; Lefebvre et al. 2014a). However, field measurements show that natural bedforms

✉ Alice Lefebvre  
alefebvre@marum.de

<sup>1</sup> MARUM – Center for Marine Environmental Sciences, University of Bremen, Leobener Str., 28359 Bremen, Germany

<sup>2</sup> HKV Consultants, P.O. Box 2120, 8203 AC Lelystad, The Netherlands

mostly display a morphology which differs from the triangular or sine-straight profiles (e.g. Carling 1996; Kostaschuk and Villard 1996; Villard and Kostaschuk 1998; Carling et al. 2000; Parsons et al. 2005; Ernstsens et al. 2006; Best et al. 2010; Kwooll et al. 2014), with stoss and lee sides having one or more brink points, i.e. breaks in the bed slope (Fig. 1a). Notably, the lee side is rarely straight; it is often composed of a relatively steep segment, the slip face, along which sediment is avalanching; upstream and/or downstream of the slip face, the bed often has a gentler slope.

Over bedforms with a straight angle-of-repose lee side, the flow separates at the crest, a reverse flow is observed above the lee side, with an eddy forming in the flow separation zone, and a turbulent wake is produced at the flow separation point, extending and expanding downstream (Engel 1981; Nelson et al. 1993; Bennett and Best 1995; Lefebvre et al. 2014a). This flow separation zone and associated turbulence production in the wake are largely responsible for the so-called form roughness, which constitutes an important part of the shear stress in environments where bedforms are present (Smith and McLean 1977; Kostaschuk and Villard 1996; Lefebvre et al. 2014b). The angle of the lee side is often thought to be a crucial component of bedform morphology because of its influence on flow: a permanent flow separation zone is present only over steep lee sides and is temporary or absent over bedforms with gentle lee sides (Kostaschuk and Villard 1996; Best and Kostaschuk 2002). Turbulence production—hence, form roughness—is therefore reduced over low-angle bedforms (which do not possess permanent flow separation)

compared to angle-of-repose bedforms (which feature a permanent flow separation zone and strong turbulent wake; Lefebvre and Winter 2016; Kwooll et al. 2016). Despite the importance of the lee side angle in shaping flow, few studies have characterised in detail flow over bedforms with lee side angles smaller than the angle of repose (Kostaschuk and Villard 1996; Best and Kostaschuk 2002; Lefebvre and Winter 2016; Kwooll et al. 2016).

Based on numerical modelling of flow over triangular bedforms, Lefebvre and Winter (2016) suggested that flow separation is permanent for lee side angles steeper than 11–18°, depending on bedform relative height. From laboratory measurements of flow over fixed bedforms, Kwooll et al. (2016) concluded that a permanent flow separation exists only over slip face angles of 30°, and a small intermittent flow separation zone is present over bedforms with slip faces of 20 and 10°. Commonly, the average slope between the crest and trough (i.e. the average angle of the lee side) has served to assess whether a flow separation zone could be present over natural bedforms (e.g. Holmes and Garcia 2008; Best et al. 2010). However, a bedform with an average lee side angle of 10° may have a steep slip face over which a permanent flow separation occurs (e.g. Kostaschuk 2000; Lefebvre et al. 2014b). Therefore, detecting only the highest and lowest elevation along the profile (i.e. crest and trough) and using them to estimate whether a flow separation zone is present could be misleading. To address this, Van der Mark and Blom (2007) suggested calculating a representative lee face slope excluding a distance of one sixth of the bedform height below the crest

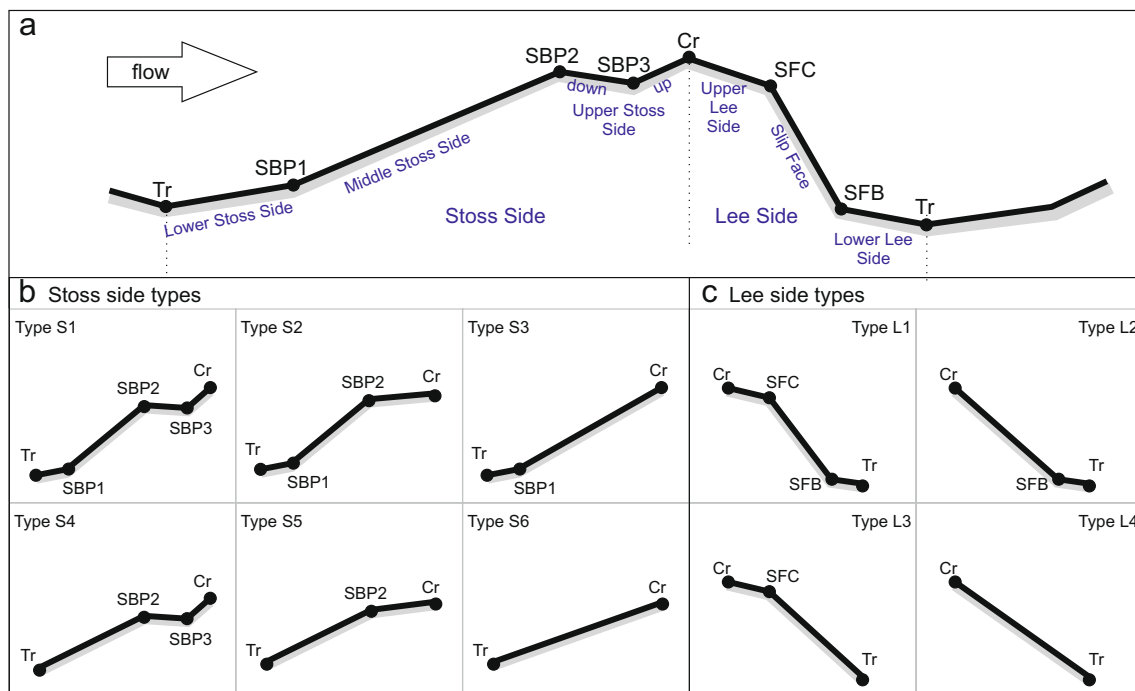


**Fig. 1** Bedform morphology: **a** bedform profile containing all possible brink points and segments; **b** stoss side types; **c** lee side types. *SBP* Stoss brink points, *SFC* slip face crest, *Cr* crest, *Tr* trough

and above the trough, arguing that these are transitional areas. This essentially removes the upper and lower lee sides of the bedforms and allows an estimation of the angle of the slip face, rather than the mean angle of the lee side. However, dimensions of “one sixth of the bedform height” may not represent the upper and lower lee sides of all bedforms; therefore, this method may not be universally applicable and could lead to incorrect values of slip face dimensions. Obviously, calculating the stoss and lee side angles (i.e. determining the position of the crest and trough and assuming a triangular shaped bedform) are not sufficient to determine the effect of a bedform on flow.

It is known that, over bedforms having a lee side composed of an upper lee side and a slip face (i.e. lee side with a brink point, Fig. 1a), the flow separates at the slip face crest and not at the bedform crest, and the length of the flow separation zone is related to the angle of the bed along the upper lee side (Kornman 1995; Paarlberg et al. 2007). Kornman (1995) further showed that an increase in the angle of the upper lee side resulted in a decrease in the flow separation length and form roughness. However, this result was based on only four laboratory experiments with bedforms having an angle-of-repose slip face. The effect of the length of the upper lee side, or of the presence and dimensions of a lower lee side (Fig. 1a) on the flow and form roughness have also never been tested. Therefore, it is hypothesised that, in order to identify whether there will be a flow separation zone, a strong wake and thus high form roughness, it is required to determine the position of the different brink points and calculate the dimensions of each segment. For example, two bedforms having similar slip faces but different dimensions of the upper and lower lee sides may or may not contribute to the same total shear stress.

Despite the potential importance of bedform morphology in determining flow, only few studies have investigated bedforms of complicated morphology (i.e. having brink points) in the laboratory (Kornman 1995; Venditti 2007; Kwohl et al. 2016) or through numerical modelling (Stoesser et al. 2008; Omidyeganeh and Piomelli 2011). This may be due to the fact that natural bedforms are of complex shape which is difficult to parameterise; no study has yet examined in detail natural bedform morphology in order to identify the different bedform features (Fig. 1a), evaluate the occurrence of morphology type (Fig. 1b and c) or calculate the relative dimensions of each morphological element. Venditti (2003) performed such an analysis on stable laboratory bedforms which, however, may not be representative of bedforms in the field; for instance, they had an angle-of-repose slip face. Therefore, there is a need to describe the geometry of natural alluvial bedforms in order to provide a basis on which to scale physical or numerical modelling of flow over bedforms.

In order to address these topics, this study aims to characterise the morphology of some natural bedforms and compare the influence on flow exerted by bedforms with a typical

natural versus an arbitrary triangular morphology. To do so, bed profiles are analysed to categorise bedform morphology. Numerical simulations of flow over bedforms with various geometries encompassing the range of shapes defined from river bed profiles are carried out. The results of the numerical simulations are used to generalise the influence of natural bedform morphology on flow and shear stress.

## Bedform morphology

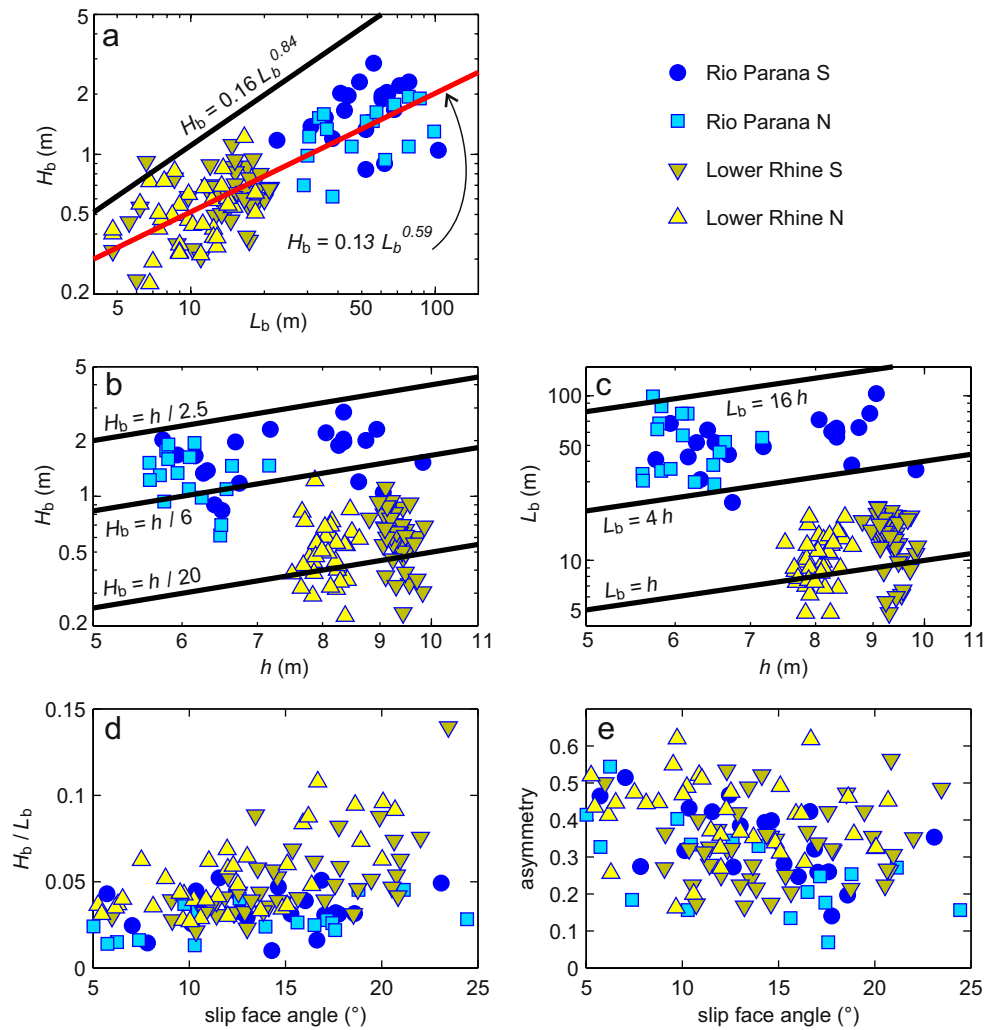
### Datasets

Data of four longitudinal bed profiles were used to characterise bedform morphology. They were extracted from two datasets of multibeam echosounder data: one from the Rio Paraná (Argentina) described in Parsons et al. (2005) and the other from the Lower Rhine (The Netherlands) reported in Frings (2007). Here, the datasets are presented briefly and the reader is referred to the original publications for more details. The two rivers have sandy sediment (fine sand in the Rio Paraná, coarse to very coarse sand in the Lower Rhine) and similar Froude numbers ( $Fr=0.12-0.15$ ).

Three-dimensional bathymetry of a section of the Rio Paraná, just upstream of the confluence of the Rio Paraguay, was measured in May 2004. The survey area was 600 m wide and 1.3 km long. The multibeam echosounder data were gridded with a grid cell of 0.5 m. Two bed profiles (referred to as Rio Paraná N and S) were extracted from the gridded data, both following the main axis of the river: one in the southern part of the survey area (shown in Figs. 2 and 3 of Parsons et al. 2005) and another one in the north. Each profile, having an average depth of 7 m, is about 1 km long and contains about 20 bedforms approx. 1.5 m high and 50 m long. The median grain size over one of the dunes was 220  $\mu\text{m}$  (Kostaschuk et al. 2009) and the average depth-averaged velocity over the length of a whole dune about 1.2  $\text{m s}^{-1}$  (Parsons et al. 2005).

A 2.3-km-long, 25-m-wide section of the Lower Rhine, situated at the IJsselkop bifurcation, was surveyed in January 2004. The measured three-dimensional bed elevations were gridded with a grid cell of 0.2 m. Two bed profiles were extracted from the gridded data, both following the main axis of the river: one in the southern part of the river, upstream of the bifurcation (Pan Kanaal, referred to as Lower Rhine S), and another in the northern part downstream of the bifurcation (Nederrijn, referred to as Lower Rhine N). Each profile is approx. 1 km long and contains 70 to 90 bedforms (bedform height 0.6 m, bedform length 15 m, water depth 9 m). The depth-averaged flow velocity during the survey was 1.1–1.4  $\text{m s}^{-1}$  and the median grain diameter 1–2 mm (Frings 2007).

**Fig. 2** Relationships between bedform height ( $H_b$ ) and length ( $L_b$ ), water depth ( $h$ ), aspect ratio ( $H_b/L_b$ ), asymmetry and slip face angle



Obviously, the datasets used here are not exhaustive and this work does not aim at characterising all possible bedform morphologies. Instead, the shape displayed by bedforms from

two unidirectional flow environments is examined and their morphology is defined in order to characterise natural bedform shape and use this information to carry out numerical

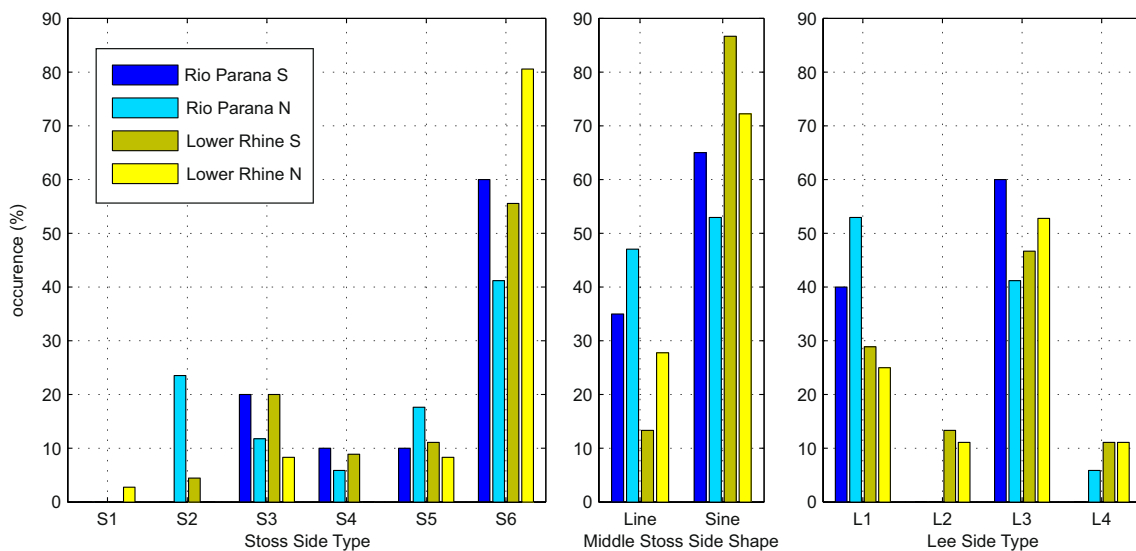


**Fig. 3** Occurrence of bedform types in the selected datasets

simulations. It also constitutes a first step towards establishing a universally applicable method to characterise bedform morphology.

### Morphology characterisation

The positions of crests and troughs of individual bedforms were determined following the bedform tracking tool developed by Van der Mark and Blom (2007). Thereafter, typical bedform features in the form of brink points marking the beginning and end of a segment of the bedform (Fig. 1a) were detected. Up to three brink points were defined on the stoss side (stoss brink points, SBP). The first of these, SBP1, separates the lower stoss side, which has a comparatively flat bed, and the middle stoss side, having a comparatively steep bed. The second stoss side brink point, SBP2, shows a change between the comparatively steep bed of the middle stoss side and the upper stoss side, which has an overall angle close to  $0^\circ$ . In those cases where the upper stoss side shows some strong variations in height, a third stoss side brink point, SBP3, separates the “down” upper slope, which has a negative angle, and the “up” upper stoss side, having a positive angle. None to three of the brink points may be present and, therefore, six stoss side types are defined (Fig. 1b).

Two brink points were defined over the lee side (Fig. 1a), the slip face crest and the slip face base, which separate the relatively flat upper and lower lee sides from the steepest part of the lee side, the slip face. The slip face is defined here as the part of the bedform lee side (i.e. between the crest and the following trough) which has angles steeper than  $5^\circ$ . In cases where the bedform slip face is composed of several segments, the slip face is taken as the longest segment with angles greater than  $5^\circ$ . The beginning and end of the slip face are the slip face crest and base. None to two lee side brink points can be present and, therefore, four lee side types are defined (Fig. 1c).

For each bedform of each profile, the occurrence and position of brink points were identified and the stoss and lee side types (as defined in Fig. 1) determined. All segments were represented by a straight line going from the crest, trough or brink point to the next brink point, crest or trough. If any segment was composed of only one point, it was joined to the neighbouring segment. The horizontal length, height and angle of each segment, as represented by this straight line, were calculated. It was also determined whether the middle stoss side was best described by a straight line or a sinusoidal curve. For this, the coefficients of determination between the original bedform profile and a profile made of a straight line or a sinusoidal wave for this segment were calculated. The middle stoss side was considered to be best represented by the shape having the highest coefficient of determination.

Some bedforms were discarded from the analysis because they had a very complicated morphology (for example, a very

large secondary bedform within their lower lee side, which could not be well described using the selected brink points) or because they had a low aspect ratio ( $H_b/L_b < 0.01$ ), no slip face (lee side angles  $< 5^\circ$ ) or a low relative bedform height ( $H_b / \text{depth} < 0.04$ ). These portions of the bed, although automatically recorded as bedforms due to bed elevation variations, were considered to represent a flat bed or secondary bedforms in case of low relative height. In total, 118 bedforms were used to characterise bedform morphology, 37 from the Rio Paraná profiles (95% of detected bedforms) and 81 from the Lower Rhine profiles (48% of detected bedforms).

### Bedform morphology

Examining at first only bedform height and length, without further exploring the morphology in detail, shows that the two datasets have different scales of bedforms, the bedforms of the Rio Paraná being larger and longer than those of the Lower Rhine (Fig. 2a). The relationship between bedform height and length is  $H_b = 0.13 L_b^{0.59}$  (coefficient of determination  $R^2 = 0.66$ , number of observations  $n = 118$ ) and falls within the upper limit defined by Flemming (1988) as  $H_{b \max} = 0.16 L_b^{0.84}$ . The two datasets are also clearly distinguished in terms of water depth, with the higher, longer bedforms of the Rio Paraná having formed in shallower water than the smaller, shorter bedforms of the Lower Rhine (Fig. 2b and c). The height and length do not exceed the upper limit of scaling of dune height and length from water depth ( $H_{b \max} = h/2.5$  and  $L_{b \max} = 16 h$ ) as reported by Venditti (2013) from the Allen (1982) dataset. However, the lower limits ( $H_{b \min} = h/20$  and  $L_{b \min} = h$ ) are noticeably too high, and the Lower Rhine bedforms are undoubtedly smaller than expected for that water depth according to these general relationships determined principally from flume-generated bedforms.

A closer look at the data shows that most of the stoss sides of the investigated bedforms are made of one segment (type S6, 62% of all considered bedforms, Fig. 3, left panel). Thereafter, the most common types are stoss sides with one brink point (types S3 and S5, respectively 15% and 11% of all considered bedforms), while types with more than one brink point occur only rarely (<6% of all considered bedforms). The middle stoss side is best described by a sinusoidal wave (74% of all considered bedforms, Fig. 3, middle panel). The lee side mainly comprises two segments, the upper stoss side and the slip face (type L3, 50% of all considered bedforms, Fig. 3, right panel). However, one third of the bedforms also show two brink points (type L1, 37%). The other two cases occur more rarely (6% for type L2 and 7% for type L4).

Most segments are very well described by straight lines (or sinusoidal in the case of the middle stoss side) between the brink points, the coefficients of determination of the different segments being generally higher than 0.85. One notable exception is the upper stoss side, with  $R^2 = 0.22$ . This is because

small, secondary bedforms are often found on the bedform upper stoss sides. As these types occur only rarely (<6% of all considered bedforms), they are not taken into account for the numerical modelling exercise.

In summary, the most typical morphological elements of the bedforms investigated here are stoss sides made of one segment with a sinusoidal shape, and lee sides made of two segments, an upper lee side and a relatively steep slip face. However, it is also quite common to have two brink points along the lee side. Despite the fact that the bedforms from the two datasets contrasted in terms of their relation of height and length to water depth, there is no obvious difference in their morphology; the stoss and lee side types, as well as the shape of the stoss side occurring most often are the same for both the Rio Paraná and the Lower Rhine.

The average bedform and segment dimensions and water depth, as well as their extreme values (5th and 95th percentiles), are presented in Table 1. Interestingly, the slip face angles never reach the angle of repose ( $30^\circ$ ), being on average  $14^\circ$ , and less than  $21^\circ$  for 95% of the bedforms; the steepest slip face determined from the present dataset has an angle of  $24.4^\circ$ . Another point to be noted is that the bedform aspect ratio ( $H_b/L_b$ ) and asymmetry ( $L_{lee}/L_b$ ), also sometimes referred to as bedform steepness, are not related to the slip face angle (Fig. 2d and e,  $R^2=0.21$  and  $0.06$  respectively). Furthermore, the height and length of the whole bedforms are interrelated as well as those of the stoss side ( $H_{SS}=0.15 L_{SS}^{0.64}$ ,  $R^2=0.80$ ,  $n=73$ ), upper lee side ( $H_{ULS}=0.03 L_{ULS}^{0.87}$ ,  $R^2=0.51$ ,  $n=98$ ), slip face ( $H_{SF}=0.25 L_{SF}^{0.92}$ ,  $R^2=0.66$ ,  $n=118$ ) and lower lee side ( $H_{LLS}=0.03 L_{LLS}^{1.09}$ ,  $R^2=0.54$ ,  $n=49$ ).

## Modelling flow over typical bedforms

### Model description

Delft3D (Deltares 2011) is a process-based open-source integrated flow and transport modelling system. In Delft3D-

FLOW the 3D nonlinear shallow water equations derived from the three-dimensional Navier–Stokes equations for incompressible free surface flow are solved. In order to capture non-hydrostatic flow phenomena such as flow recirculation on the lee of bedforms, the non-hydrostatic pressure is computed by using a pressure correction technique: for every time step, a hydrostatic step is first performed to obtain an estimate of the velocities and water levels; a second step, taking into account the effect of the non-hydrostatic pressure, is then carried out and the velocities and water levels are corrected, such that continuity is fulfilled (Deltares 2011).

The non-hydrostatic Delft3D modelling system has been used to set up a two-dimensional vertical (2DV) numerical model to simulate horizontal and vertical velocities, turbulent kinetic energy (TKE) and water levels above fixed bedforms. The model has been calibrated and validated against the laboratory flume experiments of McLean et al. (1999) and proved to correctly reproduce horizontal and vertical velocities (including flow separation), turbulence and shear stress over idealised, angle-of-repose bedforms under unidirectional flow conditions (Lefebvre et al. 2014a). Further verified against field data, the model also proved to correctly simulate velocities, TKE and water levels in a tidal environment over natural bedforms (Lefebvre et al. 2014b).

The same numerical model is used here to simulate flow over bedforms of similar dimensions as previously modelled. All simulations are performed on a 2DV plane Cartesian model grid over a fixed bed (i.e. no sediment transport) composed of 20 similar bedforms. The following conditions are prescribed constant in time at the lateral open boundaries of the model domain: a logarithmic velocity profile at the upstream boundary, and a water surface elevation of 0 m at the downstream boundary (Fig. 4). The grid sizes were set following the suggestions of Lefebvre et al. (2014a): horizontal grid size ( $dx$ ) of  $H_b/5$  ( $dx=0.18$  m for bedform height  $H_b=0.9$  m); a non-uniform vertical grid size, stretched in the vertical direction with fine spacing near the bed ( $dz_1$ ) and coarser spacing in the water column ( $dz_2$ ), whereby  $dz_1=H_b/30$  between the trough

**Table 1** Average, 5th and 95th percentile ( $p_5$  and  $p_{95}$ ) values of water depth, and bedform and segment dimensions

		Average	$p_5$	$p_{95}$
Water depth	All	8.2 m	9.6	5.8
Bedform length ( $L_b$ )	All	25.2 m	6.2	75.4
Bedform height ( $H_b$ )	All	0.9 m	0.3	2.0
Stoss side length	All	17.5 m ( $18.5 H_b$ )	3.7 ( $6.8 H_b$ )	52.8 ( $39.7 H_b$ )
Upper lee side length	L1, L3	5.5 m ( $6 H_b$ )	0.9 ( $1.5 H_b$ )	19.5 ( $15.2 H_b$ )
Upper lee side angle	L1, L3	$1.9^\circ$	$0.3^\circ$	$4.0^\circ$
Slip face length	All	3.0 m ( $3.6 H_b$ )	1.1 ( $2.1 H_b$ )	6.3 ( $6.1 H_b$ )
Slip face angle	All	$13.8^\circ$	$6.1^\circ$	$20.9^\circ$
Lower lee side length	L1, L2	1.6 m ( $1.9 H_b$ )	0.4 ( $0.5 H_b$ )	5.4 ( $7.1 H_b$ )
Lower lee side angle	L1, L2	$2.5^\circ$	$0.7^\circ$	$5.2^\circ$

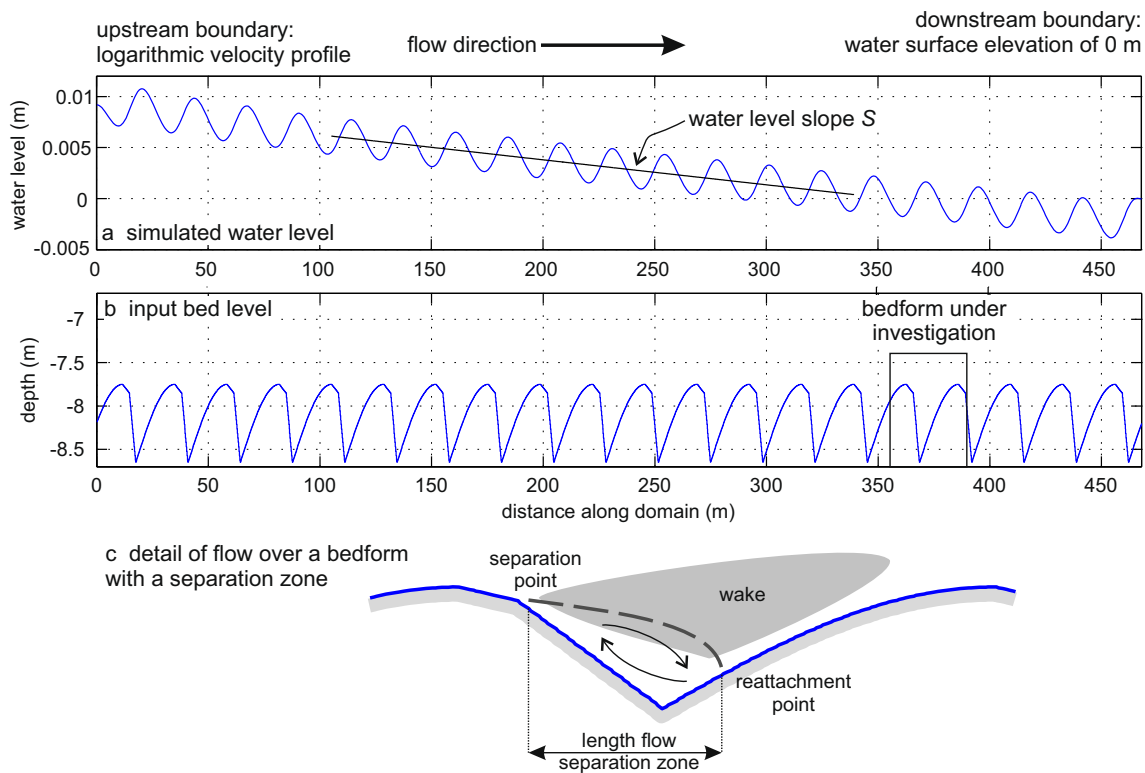


**Fig. 4** Example of simulated water level (a) over an input bed slope (b) containing 20 bedforms. c Sketch of flow over a bedform with a separation zone

position and the height of the crest  $+ 5 dz_1$ , which gradually increases to  $dz_2=0.06 h$  (where  $h$  is the water depth) within the remaining water column, resulting in 53 layers being used in each simulation. The time step is  $dt=0.001$  minutes, following a Courant Friedrich Lewy criterion  $CFL = dt \sqrt{gh} / dx < 10$  where  $dt$  is the time step and  $g$  is the acceleration due to gravity. There is a uniform background horizontal viscosity of  $10^{-3} m^2 s^{-1}$  and a background vertical eddy viscosity of  $0 m^2 s^{-1}$ , integrated into a  $k-\epsilon$  turbulence closure model (Uittenbogaard et al. 1992). Details of the model setup, calibration and validation, including the turbulence closure scheme and sensitivity to grid size, can be found in Lefebvre et al. (2014a, b).

**Simulations**

Four series of simulations were carried out to test the influence of bedform morphology on flow velocities, separation zone, turbulent kinetic energy and shear stress. For all simulations, the bedform height and length, the length of the stoss side and the water depth were taken from the dimensions calculated from typical bedform shapes; the dimensions of the upper and lower lee side and the slip face were kept within the range determined from the analysis of the natural bedform shape (Table 1). A summary of the experiments and the dimensions used is presented in Table 2.

The first series of simulations (Exp1a, Fig. 5a) examines the influence of the slip face angle on flow. This is because, over triangular bedforms, this angle determines the presence of a flow separation zone and turbulence intensity over the bedforms (Lefebvre and Winter 2016). Bedforms having a sinusoidal stoss face and a lee side made of an upper lee side and a slip face (type L3) with angles varying from  $6^\circ$  to  $24^\circ$  in  $2^\circ$  steps are modelled in order to reflect the range of slip face angles determined from bedform morphology. This experimental series is complemented by simulations reproducing some of these bedforms but with a straight stoss side instead of a sinusoidal one (Exp1b, Fig. 5b), in order to assess the influence of the stoss side shape.

The second series investigates the influence of the dimensions of the upper and lower lee side by varying first the position of the slip face crest (Exp2a, Fig. 5c) and then the position of the slip face base (Exp2b, Fig. 5d). These experiments start with a bedform having a straight lee side made of only a slip face. Keeping a constant bedform length and height, the lee side is then broken into two segments by adding a slip face crest or base, their positions being varied by increasing simultaneously the height and length of the upper or lower lee side (upper lee side length varying from 0 to 6 m by 0.5 m increments, lower lee side length varying from 0 to 3 m by 0.25 m increments). This results in a slip face angle varying from  $6.7$  to  $22.4^\circ$ , which is in the range of the  $p_5$  and  $p_{95}$  of slip face angles determined from the bed profiles (respectively  $6.1$  and  $20.9^\circ$ , Table 1).

**Table 2** Summary of bedform dimensions used for the numerical experiments. For all simulations: water depth  $h=8.2$  m, mean velocity  $u=1$  m s<sup>-1</sup>, bedform height  $H_b=0.9$  m, bedform relative height  $H_b/h=0.1$ , length stoss side=17.5 m, angle stoss side=2.9°. *Sin.* Sinusoidal

Name	Number of simulations	$L_b$ (m)	Stoss shape	Angle lee side (°)	Length upper lee side (m)	Angle upper lee side (°)	Length slip face (m)	Angle slip face (°)	Length lower lee side (m)	Angle lower lee side (°)
Exp1a	10	28.1–22.3	Sin.	4.8–10.5	3.1	1.9	7.6–1.8	6.0–24.0	0	0
Exp1b	5	28.1–22.5	Straight	4.8–10.1	3.1	1.9	7.6–2.0	6.0–22.0	0	0
Exp2a	13	25.2	Sin.	6.6	0–5.9	1.9	7.7–1.8	6.7–22.4	0	0
Exp2b	13	25.2	Sin.	6.6	3.1	1.9	4.7–1.6	9.7–22.3	0–3	2.5
Exp3	13	25.2	Sin.	6.6	4.5–2.3	1.9	2.9	14.0	0–2.5	0–2.3
Exp4	9	25.2	Sin.	6.6	3.8–4.0	0–4.0	3.8–2.3	14.0	0–0.1	5.0–0

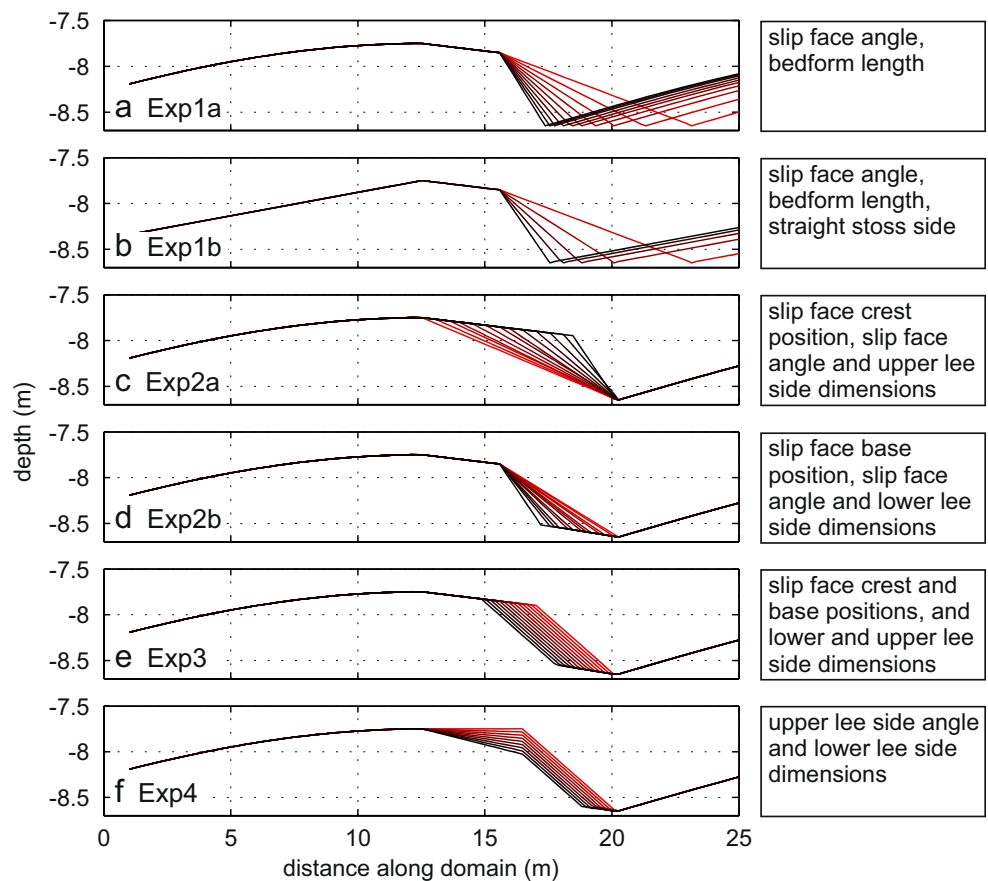
The third series is designed to determine the effect of the position of the slip face without considering the influence of the slip face angle, which is kept constant at the average value determined from the field bedform profiles (14°). The bedform lee side is made of three segments, and the slip face length and height are kept constant while the length and height of the upper and lower lee sides are simultaneously varied (Fig. 5e).

The last series of simulations tests the influence of the angle of the upper lee side. As in the third series, the angle of the slip face is kept constant at the average value determined from the field bedform profiles (14°). The angle of the slip face is

varied from 0 to 4°, whereas the length of the upper lee side is kept relatively constant, its height as well as the slip face and lower lee side dimensions being varied in order to maintain a constant bedform length and height (Fig. 5f).

In order to allow for a concise systematic study for all simulations and focus the analysis on the influence of bedform morphology, the depth-averaged water velocity at the upstream open boundary and the bed roughness were not changed between the simulations. The bed roughness was defined as a uniform roughness length  $z_0=0.0001$  m (representing a median grain diameter  $d_{50}=1.2$  mm, coarse sand). This value was chosen primarily because it is in the

**Fig. 5** Simulated bedforms, with flow from left to right; the text in the right panels describes what is varied





range where roughness length has only a small influence on the flow separation zone size and other flow properties (Lefebvre et al. 2014a); the corresponding grain size is in the range of grain size in which bedforms commonly develop, and represent typical grain sizes for the Lower Rhine (median grain diameter 1–2 mm, Frings 2007). The water velocity was set to  $1 \text{ m s}^{-1}$ , which relates to measurements of  $1.2 \text{ m s}^{-1}$  (Parsons et al. 2005) over the Rio Paraná bedforms and  $1.1\text{--}1.4 \text{ m s}^{-1}$  in the Lower Rhine (Frings 2007).

As bedform size is generally related to flow velocity and sediment size (Ashley 1990), all the bedforms simulated in this study may not represent equilibrium bedforms for the given flow and roughness conditions. However, it is known that bedforms do not adapt instantaneously to flow conditions and, therefore, bedform dimensions are not systematically representative of flow velocity; for a given flow velocity, bedforms of different sizes can be observed (Harbor 1998). Furthermore, local variations in grain size also influence bedform size and, along a channel with similar flow velocities and depth, bedforms of varying sizes can be found (Ernstsen et al. 2005). The aim of the present work is not to provide an accurate description of the mutual adjustment of flow and bedform; this is not possible since sediment transport is not modelled. Rather, it aims at providing a description of the relative effect of changes in bedform morphology on the flow. For consistency, flow velocity and bed roughness were kept the same in all simulations, although each bedform configuration would be the result of local sediment and hydrodynamic conditions. It should also be pointed out that the bedform dimensions tested here vary little in terms of height and length ( $H_b=0.9 \text{ m}$ ,  $L_b=22\text{--}28 \text{ m}$ , for a water depth of  $8.2 \text{ m}$ ), and only the bedform morphology itself is varied. The relationship between morphology and flow conditions or sediment size is currently unknown; the analysis of bed profiles from the Rio Paraná and the Lower Rhine certainly showed that different morphologies can exist along the same bed profile, which supposedly experiences similar flow conditions.

### Model output analysis

From the simulation results, the horizontal and vertical velocities and the TKE above the 16th bedform of a total of 20 bedforms are investigated in order to characterise equilibrium conditions not perturbed by entrance and exit conditions. The position and size of the flow separation zone, when present, is calculated following the method detailed in Lefebvre et al. (2014a): the flow separation line delimitates the region in which the flow going upstream (i.e. negative horizontal velocity and positive vertical velocity, below the zero-velocity line) is compensated by flow going downstream (between the zero-velocity line and the flow separation line). The length of the flow separation zone is the horizontal distance between the separation point and the reattachment point (Fig. 4c).

Because Delft3D uses the Reynolds-averaged Navier–Stokes equations, it is not possible to model intermittent flow separation; only permanent flow separation can be simulated and is considered here.

The average slope of the water level ( $S$ , calculated from bedform 5 to 15 in order to avoid inflow and outflow effects; Fig. 4a), which has adjusted to the flow conditions over the bedform field, is used to calculate the total shear stress  $\tau_T = \rho h S$  where  $\rho$  is the water density. The total shear stress is composed of the contribution of the grain shear stress and the form shear stress. The grain or flat bed shear stress is related to the input roughness length, velocity and water depth through the Chézy coefficient  $C = 18 \log(12h/30z_0) = u/\sqrt{hS}$  where  $u$  is the mean velocity. Since all simulations were carried out using the same bed roughness ( $z_0=0.0001 \text{ m}$ ), velocity ( $u=1 \text{ m s}^{-1}$ ) and water depth ( $h=8.2 \text{ m}$ ), the grain or flat bed shear stress is the same for all simulations ( $1.5 \text{ Pa}$ ). Therefore, calculating the total shear stress allows a direct comparison of the form shear stress of all the simulations.

### Model results

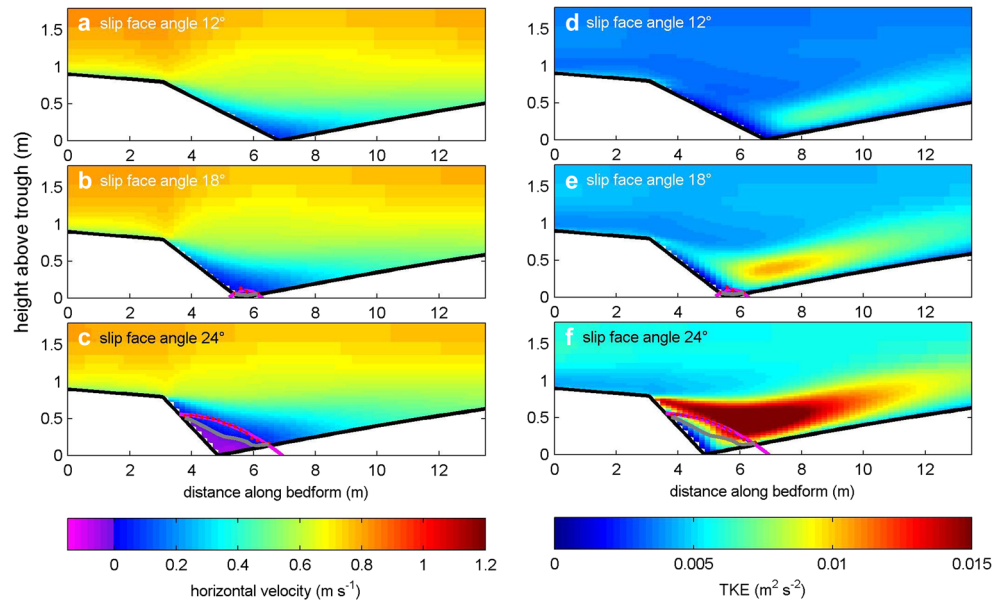
#### *Flow velocity, separation zone and turbulence*

Simulated horizontal velocities show the general pattern of flow over bedforms with flow acceleration over the stoss side and deceleration over the lee side. For slip face angles smaller than  $18^\circ$ , no flow separation occurs; a strong flow deceleration is detected over the trough but no reverse flow (e.g. Fig. 6a). For slip face angles steeper than  $18^\circ$ , the flow separation is first restricted to the trough (e.g. Fig. 6b) and becomes larger as the slip face angle increases. For a slip face angle of  $24^\circ$  (the steepest slip face tested), the flow separation zone starts just under the slip face crest and extends to a distance of  $3.6 H_{SF}$  (Fig. 6c). This is somewhat smaller than the commonly stated length of the flow separation zone over triangular or sine-straight angle-of-repose bedforms of 4 to 6  $H_b$  (Engel 1981; Lefebvre et al. 2014a), and the length of the flow separation zone over bedforms with a slip face crest and an angle-of-repose slip face of  $4.5 H_{SF}$  (Paarlberg et al. 2007). It suggests that the size of the flow separation zone would still increase for steeper slip face angles.

For small slip face angles over which there is no flow separation, the TKE along the bedform is low, with a small region of higher turbulence recognisable over the trough and stoss side (e.g. Fig. 6d). For steeper slip faces, TKE is higher and a noticeable wake is visible (e.g. Fig. 6e). At the steepest slip face tested, TKE is high with a well-defined wake extending from the crest along the flow separation line and above the following stoss side (e.g. Fig. 6f).

The presence and relative length of the flow separation zone (i.e. the length of the flow separation zone normalised

**Fig. 6** Details of horizontal velocity (left panels) and turbulent kinetic energy (TKE, right panels) over the lee side and lower stoss side of bedforms with slip face angles of 12°, 18° and 24°. Grey line Position of zero-velocity points (under which velocity is negative, i.e. flow is reversed), red dots and purple bold line position of the flow separation line (which delimitates the region in which the flow going upstream is compensated by flow going downstream)



by the height of the slip face,  $L_{FSZ}/H_{SF}$  is strongly linked to the slip face angle (Fig. 7a). For example, none of the simulations of Exp3 displays a flow separation zone because the slip face of these bedforms is smaller than 18°.

For small slip face angles, the influence of the presence of a lower lee side can also be recognised, bedforms with a slip face angle of 19° and a lower lee side (Exp2b) having no flow separation zone. Considering all simulations with bedforms having a slip face steeper than 18°, the relative length of the flow separation zone increases linearly with slip face angle ( $\theta$  in degrees), whereby  $L_{FSZ}/H_{SF}=0.55 \theta - 9.23$  ( $R^2=0.83$ ,  $n=10$ ).

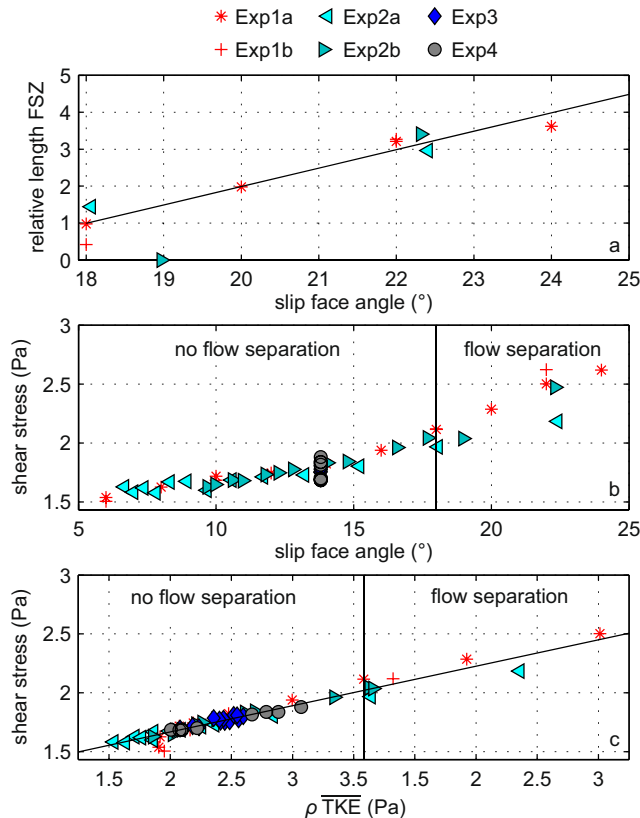


**Fig. 7** Relative length of the flow separation zone (FSZ,  $L_{FSZ}/H_{SF}$ ) as a function of slip face angle (a), and shear stress as a function of slip face angle (b) and mean TKE along the bedform (c). See Table 2 for details of the experiments

*Shear stress*

Shear stress increases with increasing slip face angle, being lowest (1.5 Pa) for the smallest slip face angle tested (6°) and highest (2.6 Pa) for the steepest face angle tested (24°; Fig. 7b). The morphology of the lee side has little influence on the shear stress; shear stress of experiments having varying slip face angles and upper and lower lee side dimensions (Exp2a and Exp2b) varies in the same range as shear stress from experiments where only the slip face angle is varied (Exp1a and Exp1b; Fig. 7b). Furthermore, the relative length of the upper and lower lee sides has very little influence on shear stress as shear stress calculated from results of Exp3 (where only the dimensions of the upper and lower lee side varied and the slip face angle was always 14°) is in the range 1.7–1.8 Pa with no particular trend (Fig. 7b).

Results from Exp4 show that the upper lee side angle has an influence on shear stress: the highest shear stress (1.9 Pa) is found for the simulation where the upper lee side angle is 0° and the slip face is the longest; shear stress decreases as the angle of the upper lee side increases, and the lowest shear stress (1.6 Pa) is found for the simulation with the steepest upper lee side angle (4°) and the shortest slip face. Finally, the shape of the stoss side has an overall small influence on shear stress which varies depending on the slip face angle: for the

small slip face angle, shear stress over bedforms with a sinusoidal stoss side is 3% (0.05 Pa) higher than over bedforms having a straight stoss side; for the highest slip face angle, shear stress is 5% (0.14 Pa) higher for the bedform with a straight stoss side than for the bedform with a sinusoidal stoss side; for the other slip face angle tested, the difference is less than 2%.

In summary, there is little influence of the length or height of the upper or lower lee side or the shape of the stoss side on form roughness; shear stress is controlled mainly by the slip face angle and, to a lesser extent, by the upper lee side angle. Similarly to shear stress, TKE intensity is principally controlled by slip face angle. As a result, a strong relation is found between mean TKE along the bedform  $\overline{\text{TKE}}$  and shear stress:  $\tau = 0.56\rho\overline{\text{TKE}} + 0.55$  ( $R^2=0.97$ ,  $n=63$ , Fig. 7c).

## Discussion

### Characterising bedform morphology

Many studies describing large bedform fields were done computing only the bedform height and length to characterise bedform properties, without detailing the bedform geometry (e.g. Harbor 1998; Van der Mark et al. 2008; Naqshband et al. 2014). Furthermore, although the curved shape of the stoss side has been widely used for laboratory and numerical modelling investigations (e.g. McLean et al. 1994; Bennett and Best 1995; Stoesser et al. 2008; Lefebvre et al. 2014a), the use of a brink point on the lee side, although often recognised from field measurements (Carling 1996; Roden 1998; Parsons et al. 2005; Ernsten et al. 2006; Lefebvre et al. 2014b), has been rarely modelled (with the exception of, for example, Venditti 2003; Kwoil et al. 2016). In fact, the present study shows that bedforms are not well represented by a triangular shape and display a variety of shapes—most typically for the bedforms analysed here, a sinusoidal stoss shape and a lee side made of two segments.

Shear stress of experiments with a lee side made of several segments varies by over 30% depending on the angle of the slip face (7–22°). All these experiments have a constant lee side angle of 7° and the variations in slip face angles are created only by varying the presence and positions of the slip face brink points. This shows that, in order to assess the influence of bedforms on flow and, in particular, the presence of reverse flow, the amount of turbulence produced and shear stress intensity, it is essential to detail the morphology of the lee side (especially whether there are brink points) and to calculate the actual angle of the different segments if present, as opposed to the average angle of the lee side or the bedform aspect ratio ( $H_b/L_b$ ) and asymmetry, as these proved not to be good proxies of slip face angles (Fig. 2d and e). Van der Mark

and Blom (2007) excluded a distance of one sixth of the bedform height below the crest and above the trough in order to compute the angle of the slip face. However, the length of the upper lee side of the bedforms investigated here measures 1.5 to 15.2  $H_b$  and the lower lee side length, when present, is 0.5 to 7.1  $H_b$ . Therefore, excluding a constant distance (of one sixth of the bedform height or other) from the lee side in order to compute the slip face dimensions is very likely to give misleading results. Instead, the bedform slip face angle needs to be determined from an analysis of bed angles calculated from high-resolution bed measurements. Calculating only the angle of the lee side would lead to erroneous assessments of whether there is a flow separation zone, how much turbulence is produced and shear stress intensity. This is particularly relevant for field studies because natural bedforms present a much more complex morphology than bedforms which form in the laboratory under controlled stable conditions.

In the present analysis of bedform shape, it has been assumed that each segment could be represented by straight lines. However, secondary bedforms are often superimposed on primary bedforms—for example, in the Rio Paraná profiles (see also Parsons et al. 2005, especially their Fig. 4). This accounts for the low coefficient of determination between a straight line and the real bed for the upper lee side. Superimposed bedforms are known to have an important effect on flow (Fernandez et al. 2006) and respond to different hydrodynamic forcing than large bedforms (Ernsten et al. 2006; Barnard et al. 2011). Therefore, future work could concentrate on determining where these secondary bedforms occur and characterising their dimensions in order to further investigate their influence on the flow and form roughness, and how they reflect hydrodynamics and sediment transport.

### Natural bedform morphology

Bedform shape is linked to the interaction of hydrodynamics and sediment transport; it is therefore expected to reflect these processes. In his study of the shape of laboratory angle-of-repose bedforms, Venditti (2003) estimated that about one third of the analysed bedforms had a brink point on the lower stoss side (SBP1). This brink point was situated 4.25 to 6.85  $H_b$  behind the preceding crest, a distance close to the range of flow separation lengths expected over angle-of-repose bedforms. He therefore suggested that the location of SBP1 was controlled by flow reattachment. Twenty-one percent of the bedforms investigated here have a brink point on the lower lee side (types S1, S2 and S3). This brink point is present behind bedforms having a relatively steep slip face of on average 16.4° (compared to a slip face angle of 13.8° on average for all bedforms). Eight occurrences of SBP1 were detected behind a slip face steeper than 18°, i.e. behind a slip face steep enough to induce flow separation; in those cases, SBP1 was situated 3.6 to 10.2  $H_{SFC}$  (on average 6.2  $H_{SFC}$ ) behind the slip

face crest. This is somewhat smaller than the expected distance between the slip face crest and the reattachment point of 8.8 to 14.4  $H_{SFC}$  (on average 10.4  $H_{SFC}$ ). Furthermore, the distance between the slip face crest and SBP1 was not related to the slip face angle ( $R^2=0.35$ ). Therefore, as a brink point has not systematically been detected at the expected position of the reattachment point, the morphology of the bedforms studied here does not suggest that the presence of a flow separation zone controls the formation of the brink point of the following stoss side.

The present analysis demonstrates that the slip face angle of the natural bedforms of the Rio Paraná and Lower Rhine never reaches an angle of repose and has a relatively low average value of  $14^\circ$ . This supports field observations (Carling 1996; Roden 1998; Carling et al. 2000; Ernstsen et al. 2005) that angle-of-repose bedforms are rarely found in natural environments. On the other hand, bedforms formed in a flume generally have steeper slip faces than natural bedforms (Van der Mark et al. 2008), which explains why angle-of-repose bedforms have been intensively studied in the laboratory. Furthermore, natural bedforms also appear to have a smaller height/length relationship to water depth than flume-formed bedforms, as suggested by Naqshband et al. (2014) and observed in the present study (Fig. 2b and c). There are therefore strong dissimilarities between the bedforms formed in a flume and in the field, which are likely due to be due to differences in hydrodynamics and sediment properties between laboratory and natural environments. Laboratory bedforms develop typically from sorted sand under steady flow conditions, which differs from natural bedforms, usually established on a bed with mixed sediment and experiencing unsteady flow conditions. The presence of cohesive sediment has been shown to alter the shape of bedforms, with bedforms having a high clay content being smaller, longer and less steep than those formed in sand alone (Schindler et al. 2015). Changes in flow conditions result in changes of bedform shape and dimensions, with a certain lag related to the time needed for bedforms to reach equilibrium with the new hydrodynamic conditions (Wilbers and Ten Brinke 2003). This also results in bedforms of different sizes being observed for a given flow condition (Harbor 1998). Differences between flume and natural bedforms may also arise from differences in scaling and ratios of, for example, sediment size, depth and flow velocity (Peakall et al. 1996).

At present, there is no known relationship between morphology and flow conditions or sediment size; there is, for example, still debate regarding the occurrence of bedforms with steep or gentle lee sides, and under which range of conditions (flow, sediment) they are formed (Best 2005). No significant differences were found between the morphology of the Rio Paraná and Lower Rhine bedforms, although they had different length and height ratios to water depth (Fig. 2). This is probably because these two environments are similar

(unidirectional flow with similar Froude number, sandy sediment); other environments may reveal dissimilarities. A characterisation of bedform shape and dimensions (including number and positions of brink points and slope of each segment) from a variety of environments (with unidirectional and tidal flows) would enable to better constrain the influence of, for example, sediment characteristics or hydrodynamics on bedform shape, and could reveal important information on the relation between bed morphology, sediment flux and flow characteristics.

### Influence of bedform morphology on flow

In the present study, flow separation was found to exist only for slip face angles steeper than  $18^\circ$ . This agrees with Lefebvre and Winter (2016), who used the same numerical model to carry out a systematic study of form friction in relation to lee side angles of triangular bedforms. The angle from which flow separation is detected agrees also with many field measurements of flow over bedforms, which suggest that permanent flow separation is present over slip faces of about  $15$ – $20^\circ$  (Ernstsen et al. 2006; Kwooll et al. 2014) but absent over slip faces of less than  $15^\circ$  (Bradley et al. 2013). A recent laboratory study (Kwooll et al. 2016) shows that intermittent flow separation exists over bedforms with slip face angles of  $10^\circ$  and  $20^\circ$  (reverse flow recorded in 2.7% and 9.4% of the cases respectively). The modelling system approach used here does not allow to simulate intermittent flow reversal, as it uses the Reynolds-averaged Navier–Stokes equations. This is certainly a shortcoming of the present work, and further study should focus on detailing *time-dependant* flow over bedforms with varying morphology.

A large-scale eddy simulation (LES) could be used for such an investigation. However, LES simulations are expensive in terms of computational time; even when carried out at laboratory scale in order to keep low Reynolds numbers, each simulation may take weeks or months (Piomelli and Omidyeganeh 2013), which is unsuitable for systematic analysis of a large number of bedform configurations. Laboratory studies can potentially circumvent this handicap by providing detailed high-frequency measurements of flow over bedforms with varying shapes and slip face angles. In particular, flume measurements allow to characterise flow intermittency (Best and Kostaschuk 2002; Kwooll et al. 2016). However, limitations also exist for that approach: the number of bed configurations which can be tested is still limited as it takes time and effort to build each bedform prototype and measure flow over them at high resolution; scaling of bedforms can be problematical (cf. Froude numbers are generally much higher in the flume than in the field); more importantly, it is difficult to get reliable measurements near the bed, especially in the bedform trough where the highest intermittency values occur (Kwooll et al. 2016). Therefore, numerical and laboratory studies

should ideally be used to complement each other, as both have advantages and disadvantages.

For given angles of each segment, the length and height of the upper and lower lee sides do not have such a strong influence on shear stress values. However, the angle of the upper lee side does have an effect on shear stress, which agrees with results from Kornman (1995) who concluded that form roughness is reduced considerably when the angle of the upper lee side increases. His experiments were carried out with bedforms having an angle-of-repose slip face. The numerical experiments confirm his results over low-angle bedforms; the shear stress of the bedforms with an upper lee side angle of 0° is 12% higher than that of bedforms with an upper lee side angle of 4°.

The results from Kwooll et al. (2016) differ from those of the present study in that the former imply that there is no permanent flow separation (>50% of the cases) for slip face angles of 20°. However, there is an agreement in that, for relatively gentle slip faces (18–20°), flow separation is constrained in the bedform trough; over steeper slip faces, the flow separates at the slip face crest. Furthermore, both studies conclude that turbulence and shear stress increase with increasing slip face angles. Kwooll et al. (2016) estimated that the nonlinear increase in shear stress with slip face angle reflected nonlinear variations in the turbulent flow field. In the present study, the strong linear relation identified between turbulence and shear stress (Fig. 7c) further suggests that variations in shear stress with slip face angle are controlled by variations in turbulence. The ratio of total shear stress to shear stress over a flat bed ( $\tau_T/\tau_S$ ) of the numerical simulations shows a very good agreement to the laboratory measurements of Kwooll et al. (2016) above bedforms with similar aspect ratios ( $H_b/L_b=0.03$  and relative height  $H_b/h=0.15$ ). The increase of  $\tau_T/\tau_S$  with slip face angle also follows the equations proposed by Kwooll et al. (2016; Fig. 8,  $R^2=0.90$ ,  $n=66$ ):

$$\tau_T/\tau_S = 1 + 0.001\theta_{SF}^2 \tag{1}$$

Although providing a good and simple fit to the data, Eq. 1 may not be appropriate as it implies an accelerating increase of shear stress with slip face angle. In reality, shear stress is likely to reach a plateau around 30° (Ogink 1989; Van Rijn 1993; Lefebvre and Winter 2016). The type of equation proposed by Lefebvre and Winter (2016) for the increase of form friction with slip face angle describes such a pattern and also well fits the data from the present study and from the Kwooll et al. (2016) laboratory results (Fig. 8,  $R^2=0.92$ ,  $n=66$ ):

$$\tau_T/\tau_S = \frac{1}{1 + e^{-0.2\theta_{SF}+4.1}} + 1 \tag{2}$$

Both Eqs. 1 and 2 are, however, unlikely to be universal, as shear stress varies not only with slip face angle but also with

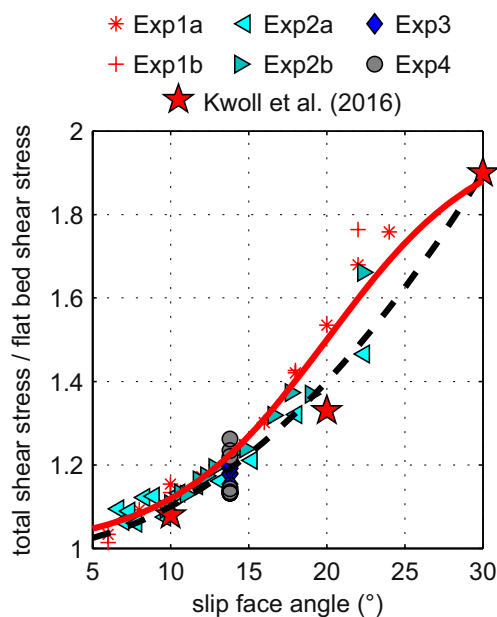


**Fig. 8** Ratio of the shear stress associated with a flat bed at the velocity and depth without bedforms and the shear stress calculated from the model simulation results as a function of slip face angle; see Table 2 for details of the experiments. *Dashed line* Approximation of Eq. 1, *solid line* Eq. 2

aspect ratio and relative height (Lefebvre et al. 2014a; Lefebvre and Winter 2016). Nevertheless, they provide an estimate of the relative contribution of bedform roughness to shear stress. Total shear stress over bedforms having the dimensions modelled here (Table 2) and with a slip face angle of 14° (the average angle of the bedforms analysed in this study) is 13 to 26% higher than that of a flat bed; assuming that  $\tau_T/\tau_S$  over such bedforms having a 30° slip face follows that of Kwooll et al. (2016), total shear stress is reduced by about 70 to 85% over bedforms with a slip face angle of 14° compared to angle-of-repose bedforms. Therefore, natural low-angle bedforms are likely to provide a greater roughness than a flat bed, albeit not as high as usually assumed in previous work on angle-of-repose bedforms. It should also be noted that bedforms having a slip face angle smaller than ~8° have a shear stress which is less than 10% higher than the shear stress over a flat bed (Fig. 8). Therefore, those bedforms which have a very low slip face angle should not be considered as additional roughness elements.

Future research should concentrate on characterising flow and roughness over bedforms with slip face angles of 10–20°. These constitute 70% of the bedforms determined from the bed profiles, and they are therefore likely to be frequently found in natural environments. The mutual adjustment of flow, sediment transport and bed morphology over these bedforms is still poorly constrained; the exact processes of intermittent and permanent flow separation, and associated turbulence should be further investigated as well as the processes creating such bedform morphology.

## Conclusions

High-resolution bed profiles from two alluvial environments were analysed to characterise natural bedform morphology. The most common morphological elements were a stoss side made of a single sinusoidal segment and a lee side composed of two segments, a gently sloping upper lee side and a relatively steep slip face. Lee sides made of three segments were also fairly common. The slip face angles never reached the angle of repose and were in the range of 6–21°.

Numerical simulations were carried out to determine how bedform shape, through the occurrence and dimensions of these segments, influences flow and shear stress over bedforms. Results show that the occurrence and length of a flow separation zone were mainly determined by the slip face angle. For the bedform dimensions tested here, no flow separation was detected for slip face angles smaller than 18°. For slip face angles steeper than 18°, the size of the flow separation zone increases with increasing slip face angle. The shear stress is principally influenced by the slip face angle and little affected by the dimensions or positions of the upper and lower lee sides. However, shear stress decreases with increasing angle of the upper lee side. Turbulence and shear stress are strongly linked, shear stress increasing linearly with the average TKE above the bedform. Therefore, in order to correctly estimate the presence of a flow separation zone and the intensity of turbulence and shear stress over bedforms, it is necessary to detail the bedform shape, in particular the presence and location of brink points on the lee side and the angle of the slip face, and not only determine the position of the bedform crest and trough and assume a triangular shape.

This work contributes to the characterisation of typical bedform morphology and provides a method to determine bedform characteristics from bed profiles. Further studies should complement it in order to further elaborate the relation between bed morphology and flow and sediment properties. It is important to note that the average slip face angle determined from the bed profiles is 14°, over which there is no permanent flow separation, and shear stress and turbulence are higher than over a flat bed but much lower than over angle-of-repose bedforms. Therefore, it is likely to be inaccurate to assume high shear stress simply due to the presence of bedforms. Instead, the slip face angle should be determined in order to correctly parameterise the influence of bedforms on flow.

**Acknowledgements** This study was funded through the DFG Research Center/Cluster of Excellence “The Ocean in the Earth System”. Alice Lefebvre is appreciative of the support provided by GLOMAR – Bremen International Graduate School for Marine Sciences. The authors wish to thank Roy M. Frings and Daniel R. Parsons for providing the multibeam echosounder data used in the analysis. Eva Kwoell is also thanked for giving helpful suggestions on the structure of the discussion. Three reviewers are acknowledged for comments on an earlier version of

the article, as well as the journal editors for other suggestions. Data are available through the Publishing Network for Geoscientific & Environmental Data (PANGAEA, <http://www.pangaea.de>).

## Compliance with ethical standards

**Conflict of interest** The authors declare that there is no conflict of interest with third parties.

## References

- Allen JRL (1982) Sedimentary structures: their character and physical basis. Elsevier, New York
- Ashley GM (1990) Classification of large-scale subaqueous bedforms: a new look at an old problem. *J Sediment Res* 60:160–172. doi:10.2110/JSR.60.160
- Barnard PL, Erikson LH, Kvitek RG (2011) Small-scale sediment transport patterns and bedform morphodynamics: new insights from high-resolution multibeam bathymetry. *Geo-Mar Lett* 31:227–236. doi:10.1007/s00367-011-0227-1
- Bennett SJ, Best JL (1995) Mean flow and turbulence structure over fixed, two-dimensional dunes: implications for sediment transport and bedform stability. *Sedimentology* 42:491–513. doi:10.1111/j.1365-3091.1995.tb00386.x
- Best J (2005) The fluid dynamics of river dunes: a review and some future research directions. *J Geophys Res Earth Surf* 110:F04S02. doi:10.1029/2004JF000218
- Best J, Kostaschuk R (2002) An experimental study of turbulent flow over a low-angle dune. *J Geophys Res Oceans* 107:3135. doi:10.1029/2000JC000294
- Best J, Simmons S, Parsons D, Oberg K, Czuba J, Malzone C (2010) A new methodology for the quantitative visualization of coherent flow structures in alluvial channels using multibeam echo-sounding (MBES). *Geophys Res Lett* 37, L06405. doi:10.1029/2009GL041852
- Bradley RW, Venditti JG, Kostaschuk R, Church MA, Hendershot M, Allison MA (2013) Flow and sediment suspension events over low-angle dunes: Fraser Estuary, Canada. *J Geophys Res* 118: 1693–1709. doi:10.1002/jgrf.20118
- Carling PA (1996) Morphology, sedimentology and palaeohydraulic significance of large gravel dunes, Altai Mountains, Siberia. *Sedimentology* 43:647–664. doi:10.1111/j.1365-3091.1996.tb02184.x
- Carling PA, Golz E, Orr HG, Radecki-Pawlik A (2000) The morphodynamics of fluvial sand dunes in the River Rhine, near Mainz, Germany. I. Sedimentology and morphology. *Sedimentology* 47:227–252. doi:10.1046/j.1365-3091.2000.00290.x
- Deltares (2011) User manual Delft3D-FLOW. Deltares, Delft, The Netherlands
- Engel P (1981) Length of flow separation over dunes. *J Hydraul Div* 107: 1133–1143
- Ernstsen VB, Noormets R, Winter C, Hebbeln D, Bartholomae A, Flemming BW, Bartholdy J (2005) Development of subaqueous barchanoid-shaped dunes due to lateral grain size variability in a tidal inlet channel of the Danish Wadden Sea. *J Geophys Res Earth Surf* 110:F04S08. doi:10.1029/2004JF000180
- Ernstsen VB, Noormets R, Winter C, Hebbeln D, Bartholomä A, Flemming BW, Bartholdy J (2006) Quantification of dune dynamics during a tidal cycle in an inlet channel of the Danish Wadden Sea. *Geo-Mar Lett* 26:151–163. doi:10.1007/s00367-006-0026-2

- Fernandez R, Best J, López F (2006) Mean flow, turbulence structure, and bed form superimposition across the ripple-dune transition. *Water Resour Res* 42, W05406. doi:10.1029/2005WR004330
- Flemming BW (1988) On the classification of subaquatic flow-transverse bedforms (in German). *Bochum Geol Geotech Arb* 29:44–47
- Frings RM (2007) From gravel to sand. Downstream fining of bed sediments in the lower river Rhine. PhD thesis, Utrecht University. Netherlands Geographical Studies 368, Royal Dutch Geographical Society, Utrecht, The Netherlands
- Harbor DJ (1998) Dynamics of bedforms in the lower Mississippi River. *J Sediment Res* 68:750–762. doi:10.2110/jsr.68.750
- Holmes RR Jr, Garcia MH (2008) Flow over bedforms in a large sand-bed river: a field investigation. *J Hydraul Res* 46:322–333. doi:10.3826/jhr.2008.3040
- Kornman BA (1995) The effect of changes in the lee shape of dunes on the flow field, turbulence, and hydraulic roughness. Report R 95-1, University of Utrecht, Utrecht, The Netherlands
- Kostaschuk R (2000) A field study of turbulence and sediment dynamics over subaqueous dunes with flow separation. *Sedimentology* 47: 519–531. doi:10.1046/j.1365-3091.2000.00303.x
- Kostaschuk R, Villard P (1996) Flow and sediment transport over large subaqueous dunes: Fraser River, Canada. *Sedimentology* 43:849–863. doi:10.1111/j.1365-3091.1996.tb01506.x
- Kostaschuk R, Shugar D, Best J, Parsons D, Lane S, Hardy R, Orfeo O (2009) Suspended sediment transport and deposition over a dune: Río Paraná, Argentina. *Earth Surf Process Landf* 34:1605–1611. doi:10.1002/esp.1847
- Kwoll E, Becker M, Winter C (2014) With or against the tide: the influence of bedform asymmetry on the formation of macroturbulence and suspended sediment patterns. *Water Resour Res* 50:7800–7815. doi:10.1002/2013WR014292
- Kwoll E, Venditti JG, Bradley RW, Winter C (2016) Flow structure and resistance over subaqueous high- and low-angle dunes. *J Geophys Res Earth Surf* 121:545–564. doi:10.1002/2015JF003637
- Lefebvre A, Winter C (2016) Predicting bed form roughness: the influence of lee side angle. *Geo-Mar Lett* 36:121–133. doi:10.1007/s00367-016-0436-8
- Lefebvre A, Paarlberg AJ, Winter C (2014a) Flow separation and shear stress over angle of repose bedforms: a numerical investigation. *Water Resour Res* 50:986–1005. doi:10.1002/2013WR014587
- Lefebvre A, Paarlberg AJ, Ernstsens VB, Winter C (2014b) Flow separation and roughness lengths over large bedforms in a tidal environment: a numerical investigation. *Cont Shelf Res* 91:57–69. doi:10.1016/j.csr.2014.09.001
- McLean SR, Nelson JM, Wolfe SR (1994) Turbulence structure over two-dimensional bed forms: implications for sediment transport. *J Geophys Res* 99:12729–12747. doi:10.1029/94JC00571
- McLean SR, Wolfe SR, Nelson JM (1999) Spatially averaged flow over a wavy boundary revisited. *J Geophys Res* 104:15743–15753. doi:10.1029/1999JC900116
- Naqshband S, Ribberink J, Hulscher S (2014) Using both free surface effect and sediment transport mode parameters in defining the morphology of river dunes and their evolution to upper stage plane beds. *J Hydraul Eng* 140:06014010. doi:10.1061/(ASCE)HY.1943-7900.0000873
- Nelson JM, McLean SR, Wolfe SR (1993) Mean flow and turbulence fields over two-dimensional bed forms. *Water Resour Res* 29:3935–3953. doi:10.1029/93WR01932
- Ogink H (1989) Hydraulic roughness of single and compound bed forms. Part XI. Report on model investigations. Delft Hydraulics Laboratory, Delft, The Netherlands
- Omidyeganeh M, Piomelli U (2011) Large-eddy simulation of two-dimensional dunes in a steady, unidirectional flow. *J Turbul* 12:1–31. doi:10.1080/14685248.2011.609820
- Paarlberg AJ, Dohmen-Janssen CM, Hulscher SJMH, Termes P (2007) A parameterization of flow separation over subaqueous dunes. *Water Resour Res* 43, W12417. doi:10.1029/2006WR005425
- Parsons DR, Best JL, Orfeo O, Hardy RJ, Kostaschuk R, Lane SN (2005) Morphology and flow fields of three-dimensional dunes, Río Paraná, Argentina: results from simultaneous multibeam echo sounding and acoustic Doppler current profiling. *J Geophys Res* 110:F04S03. doi:10.1029/2004JF000231
- Peakall J, Ashworth PJ, Best JL (1996) Physical modelling in fluvial geomorphology: principles, applications and unresolved issues. In: Rhoads BL, Thorne CE (eds) *The scientific nature of geomorphology*. Wiley, New York, pp 221–253
- Piomelli U, Omidyeganeh M (2013) Large-eddy simulations in dune-dynamics research. In: Van Lancker V, Garlan T (eds) *MARID 2013 4th Int Conf Marine and River Dune Dynamics*, Bruges, Belgium. VLIZ Spec Publ 65, pp 15–22
- Roden JE (1998) The sedimentology and dynamics of mega-dunes, Jamuna River, Bangladesh. PhD thesis, University of Leeds, Leeds, UK
- Schindler RJ, Parsons DR, Ye L, Hope JA, Baas JH, Peakall J, Manning AJ, Aspden RJ, Malarkey J, Simmons S, Paterson DM, Lichtman ID, Davies AG, Thorne PD, Bass SJ (2015) Sticky stuff: redefining bedform prediction in modern and ancient environments. *Geology* 43:399–402. doi:10.1130/G36262.1
- Smith JD, McLean SR (1977) Spatially averaged flow over a wavy surface. *J Geophys Res* 84:1735–1746. doi:10.1029/JC082i012p01735
- Stoesser T, Braun C, Garcia-Villalba M, Rodi W (2008) Turbulence structures in flow over two-dimensional dunes. *J Hydraul Eng* 134:42–55. doi:10.1061/(ASCE)0733-9429(2008)134:1(42)
- Uittenbogaard R, van Kester J, Stelling G (1992) Implementation of three turbulence models in 3D-TRISULA for rectangular grids. Tech Rep Z81, WL. Delft Hydraulics, Delft, The Netherlands
- Van der Mark CF, Blom A (2007) A new and widely applicable tool for determining the geometric properties of bedforms. University of Twente, Enschede
- Van der Mark CF, Blom A, Hulscher SJMH (2008) Quantification of variability in bedform geometry. *J Geophys Res* 113, F03020. doi:10.1029/2007JF000940
- Van Rijn LC (1993) Principles of sediment transport in rivers, estuaries and coastal seas. Aqua Publications, Amsterdam
- Venditti JG (2003) Initiation and development of sand dunes in river channels. PhD thesis, University of British Columbia, Vancouver, Canada
- Venditti JG (2007) Turbulent flow and drag over fixed two- and three-dimensional dunes. *J Geophys Res* 112, F04008. doi:10.1029/2006JF000650
- Venditti JG (2013) Bedforms in sand-bedded rivers. In: Shroder J, Wohl E (eds) *Treatise on geomorphology*. Academic Press, San Diego, pp 137–162. doi:10.1016/B978-0-12-374739-6.00235-9
- Venditti JG, Bennett SJ (2000) Spectral analysis of turbulent flow and suspended sediment transport over fixed dunes. *J Geophys Res* 105: 22035–22047. doi:10.1029/2000JC900094
- Villard P, Kostaschuk R (1998) The relation between shear velocity and suspended sediment concentration over dunes: Fraser Estuary, Canada. *Mar Geol* 148:71–81. doi:10.1016/S0025-3227(98)00015-2
- Wilbers AWE, Ten Brinke WBM (2003) The response of subaqueous dunes to floods in sand and gravel bed reaches of the Dutch Rhine. *Sedimentology* 50:1013–1034. doi:10.1046/j.1365-3091.2003.00585.x